PROCEEDINGS OF SCIENCE

Recent highlights from the LHCb experiment

Mark Whitehead[a,*]

[a] *University of Glasgow, Glasgow, Scotland*

E-mail: Mark.Whitehead@Glasgow.ac.uk

A summary of recent highlights from the LHCb experiment at CERN is presented. A range of topics are covered, including the flavour anomalies in semi-leptonic b-hadron decays and heavy flavour spectroscopy, including several first observations of new (exotic) hadrons.

The 41st International Symposium on Lattice Field Theory (LATTICE2024)
28 July - 3 August 2024
Liverpool, UK

*Speaker

https://pos.sissa.it/

PoS(LATTICE2024)003

1. Introduction

The Large Hadron Collider beauty (LHCb) experiment [1] is based at point 8 of the Large Hadron Collider at CERN. The results presented in this recent overview are based on data samples collected during LHC Run 1 (2011-2012) and Run 2 (2015-2018) in proton-proton collisions at centre-of-mass energies of 7 and 13.5 TeV, respectively. The focus of this review are topics of interest to the Lattice QCD community, namely semi-leptonic b hadron decays and heavy flavour spectroscopy.

2. Lepton flavour universality

Lepton flavour universality derives from the fact that the weak interaction is expected to couple to the three generations of leptons in the same way, once the different masses are taken into account. Recent results from the LHCb collaboration and the B-factory experiments have showed some tension with standard model predictions at the level of about 3σ. Such measurements consider the ratio of semi-leptonic b-hadron decays defined as

$$R(D) = \frac{\mathcal{B}(\bar{B} \to D\tau^- \bar{\nu_\tau})}{\mathcal{B}(\bar{B} \to D\mu^- \bar{\nu_\mu})} \text{ and } R(D^*) = \frac{\mathcal{B}(\bar{B} \to D^*\tau^- \bar{\nu_\tau})}{\mathcal{B}(\bar{B} \to D^*\mu^- \bar{\nu_\mu})}. \tag{1}$$

2.1 $R(D^+)$ and $R(D^{*+})$

The recent result from the LHCb experiment describing a simultaneous measurement of $R(D^+)$ and $R(D^{*+})$ is described in detail in Ref. [2]. It uses the 2015-2016 sub-dataset from LHCb Run 2 and considers the following four processes: $B \to D^+\mu^-\nu_\mu$, $B \to D^+\tau^- (\to \mu^-\bar{\nu}_\mu\nu_\tau)\,\nu_\tau$, $B \to D^{*+} (\to D^+\pi^0)\,\mu^-\nu_\mu$ and $B \to D^{*+} (\to D^+\pi^0)\,\tau^- (\to \mu^-\bar{\nu}_\mu\nu_\tau)\,\nu_\tau$. Note that the neutrinos and neutral pions are not reconstructed, so there is a single data sample containing the $D^+\mu^-$ candidates.

In addition to the four signal processes, there are several background contributions. Firstly, from B mesons decays with two charm hadrons in the final state $B \to D^+X_cX$ where X is a particle and X_c a charmed particle. Semi-leptonic decays from higher excited charm states also contribute, $B \to D^{**}\mu^-\nu_\mu$ and $B \to D^{**}\tau^-\nu_\tau$ with D^{**} one of many possible excited charm meson states. Further components are combinatorial background where unrelated tracks are wrongly combined into the D and B meson candidates and from misidentified backgrounds where other particles are wrongly identified as a muon.

Three-dimensional templated fits are used to extract the yields of each component, these are q^2, m^2_{miss} and E^*_μ. Here q^2 is the momentum of the lepton pair from the B meson decay, m^2_{miss} is the missing mass squared from the neutral pions and neutrinos that are not reconstructed and E^*_μ is the energy of the muon in the B meson result frame. The fit results are shown in Fig. 1 and the extracted yields give

$$R(D^+) = 0.249 \pm 0.043 \pm 0.047, \tag{2}$$
$$R(D^{*+}) = 0.402 \pm 0.081 \pm 0.085, \tag{3}$$

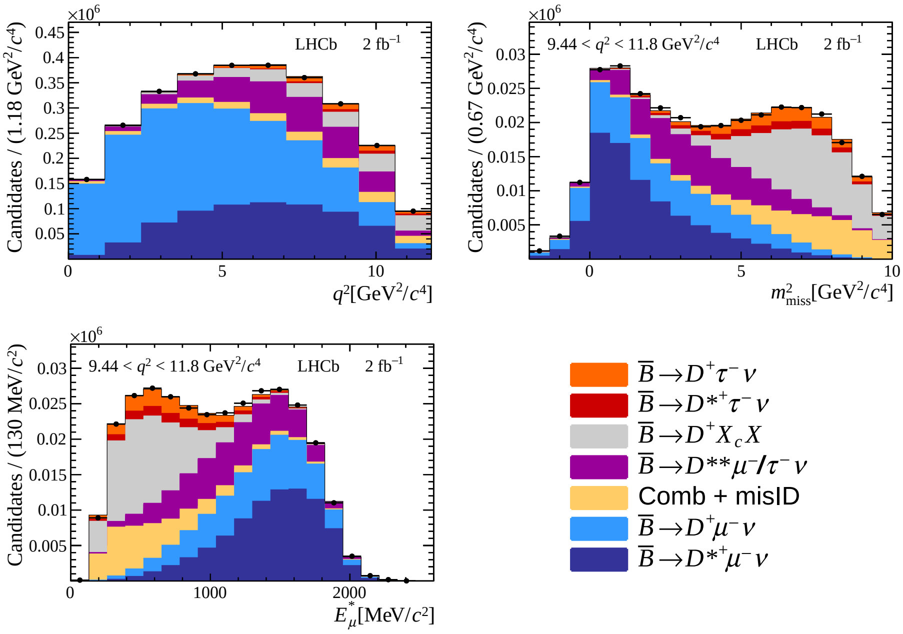

Figure 1: Projections of the fit in (top left) q^2, (top right) m^2_{miss} and (bottom left) E^*_μ. The different components are described in the legend. Taken from Ref [2].

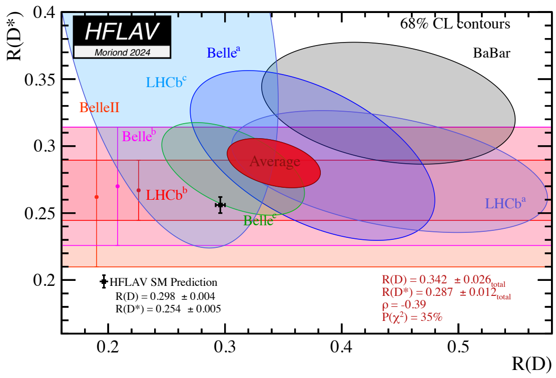

Figure 2: Results of a combination of measurements of $R(D)$ and $R(D^*)$, with the average in bold red and the SM prediction as the black point with error bars. Taken from Ref. [3].

where the first uncertainty is statistical and the second systematic. These new results are included in the HFLAV average [3] shown in Fig. 2, where the tension with the standard model prediction remains at the 3σ level.

Future prospects to improve the precision of the results are promising, with LHCb Run 2 data from 2017 and 2018 available, as well as the new Run 3 data sample from 2024. The dominant systematic uncertainty sources, form factors, background fractions, and simulation statistics should all be reducible to take advantage of the increased statistical power available.

PoS(LATTICE2024)003

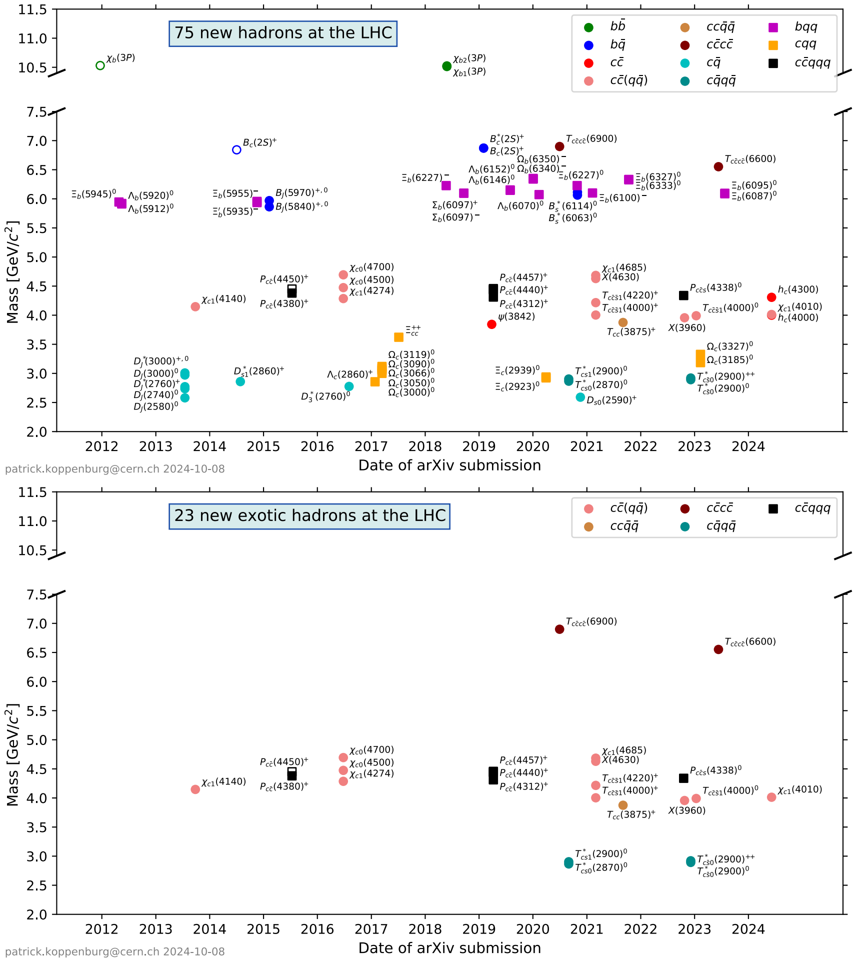

Figure 3: Summary of hadrons discovered at the LHC with a focus (right) on exotic candidates. Reproduced from Ref [4].

3. Spectroscopy

Heavy flavour spectroscopy remains a hot topic in particle physics, following a revival by the huge number of hadrons that are being discovered at the LHC. Figure 3 summarises the discoveries, with (top) a total of 75 new hadrons including (bottom) 23 that seems to be exotic in nature (not standard mesons or baryons). Three recent results from LHCb are summarised below, that found a total of 5 new states.

3.1 Amplitude analysis of $B^0 \to \bar{D}^0 D_s^+ \pi^-$ and $B^+ \to D^- D_s^+ \pi^+$ decays

The amplitude analysis of $B^0 \to \bar{D}^0 D_s^+ \pi^-$ and $B^+ \to D^- D_s^+ \pi^+$ decays is described in detail in Refs. [5, 6]. The motivation to study these channels is the observation of the $T^*_{cs0}(2870)^0$ and $T^*_{cs1}(2900)^0$ states in $B^- \to D^- D^+ K^-$ [7, 8] decays, which are tetraquark candidates with minimum quark content $cs\bar{u}\bar{d}$. The tetraquark candidates were observed in the $D^+ K^-$ channel, so it is well motivated to study the $D_s^+ \pi^\pm$ channels which have the same quark flavours but a different arrangement of quarks and antiquarks.

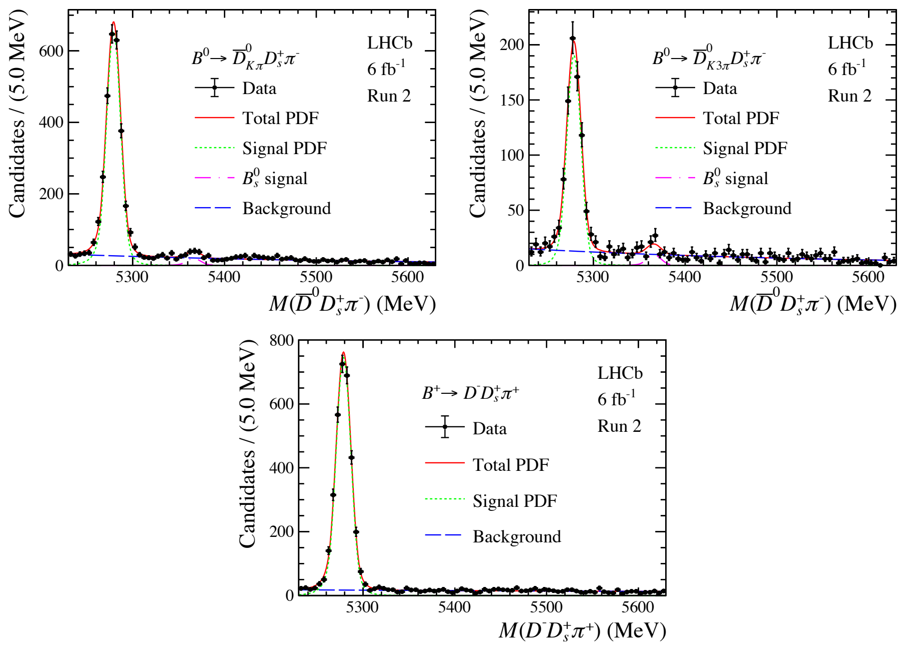

Figure 4: Fits to the B candidate invariant mass distribution for (top left) $B^0 \to \bar{D}^0 D_s^+ \pi^-$ with $\bar{D}^0 \to K^+\pi^-$, (top right) $B^0 \to \bar{D}^0 D_s^+ \pi^-$ with $\bar{D}^0 \to K^+\pi^-\pi^+\pi^-$ and (bottom) $B^+ \to D^- D_s^+ \pi^+$ decays using Run 2 data. The components are as described in the legend, figures reproduced from Ref. [5].

The $B^0 \to \bar{D}^0 D_s^+ \pi^-$ channel is reconstructed using both $\bar{D}^0 \to K^+\pi^-$ and $\bar{D}^0 \to K^+\pi^-\pi^+\pi^-$ decays. The $B^+ \to D^- D_s^+ \pi^+$ is reconstructed with $D^- \to K^+\pi^-\pi^-$ decays and both channels require $D_s^+ \to K^+K^-\pi^+$. This analysis uses the full Run 1 and Run 2 data samples. The two main sources of background, random combinations of tracks and final states without two correctly reconstructed charm mesons, are removed using a boosted decision tree algorithm and requirements on the flight distance of the charm meson candidates, respectively. Following the selection, candidates in the Run 2 data samples can be seen with the result of an extended maximum likelihood fit superimposed in Fig. 4. This fit to the B candidate invariant mass distribution is used to determine the signal and background yields in a 20 MeV window around the known B-meson mass to be used in the amplitude analysis. In total there are approximately 4000 signal candidates in each B meson decay mode, with total background contributions below the 10% level.

The first step for the amplitude analysis is to try to fit the data using the known D^{**} mesons in the $m(\bar{D}^0\pi^-)$ and $m(D^-\pi^+)$ channels for the $B^0 \to \bar{D}^0 D_s^+ \pi^-$ and $B^+ \to D^- D_s^+ \pi^+$ candidates, respectively. These are summarised in Fig. 5, and the projections of the fit model to the data samples is illustrated in Fig 6. The projections onto $m(\bar{D}^0\pi^-)$ and $m(D^-\pi^+)$ show the fit model of D^{**} mesons reproduces the data very well, however the $m(D_s^+\pi^-)$ and $m(D_s^+\pi^+)$ distributions show some discrepancies in the peak and dip region between 2.8 and 3.2 GeV. Therefore some tetraquark candidates were added to the fit model, the results of a configuration including a spin 0 tetraquark in both $m(D_s^+\pi^-)$ and $m(D_s^+\pi^+)$ channels simultaneously are shown in Fig. 7. The fit results from the full fit model including the tetraquark candidates shows a significant improvement in the fit quality.

Resonance	J^P	Mass (GeV)	Width (GeV)	Comments
$\overline{D}^*(2007)^0$	1^-	2.00685 ± 0.00005	$< 2.1 \times 10^{-3}$	Width set to be 0.1 MeV
$D^*(2010)^-$	1^-	2.01026 ± 0.00005	$(8.34 \pm 0.18) \times 10^{-5}$	
$\overline{D}_0^*(2300)$	0^+	2.343 ± 0.010	0.229 ± 0.016	#
$\overline{D}_2^*(2460)$	2^+	2.4611 ± 0.0007	0.0473 ± 0.0008	#
$\overline{D}_1^*(2600)^0$	1^-	2.627 ± 0.010	0.141 ± 0.023	#
$\overline{D}_3^*(2750)$	3^-	2.7631 ± 0.0032	0.066 ± 0.005	#
$\overline{D}_1^*(2760)^0$	1^-	2.781 ± 0.022	0.177 ± 0.040	#
$\overline{D}_J^*(3000)^0$	$?^?$	3.214 ± 0.060	0.186 ± 0.080	# $J^P = 4^+$ is assumed

Figure 5: Details of the various D^{**} resonances included in the fit models, from Ref [5].

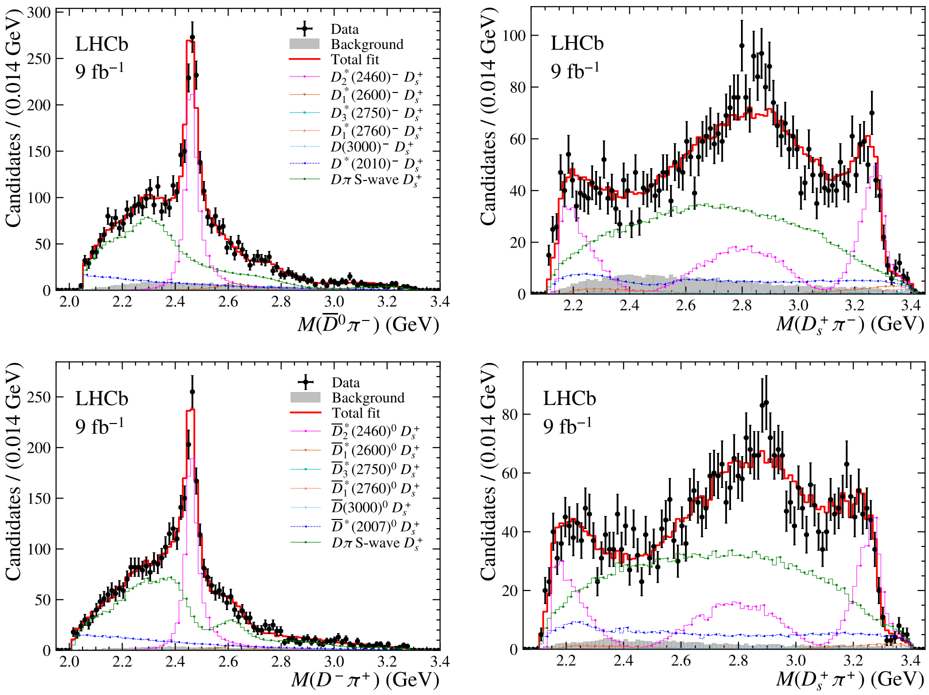

Figure 6: Fit projections of the D^{**}-only fit model for (top left) $m(\bar{D}^0\pi^-)$ and (top right) $m(D_s^+\pi^-)$ for $B^0 \to \bar{D}^0 D_s^+\pi^-$ decays, and (bottom left) $m(D^-\pi^+)$ and (bottom right) $m(D_s^+\pi^+)$ for $B^+ \to D^- D_s^+\pi^+$ decays for Run 1 and Run 2 datasets combined. Fit components are as described in the legend, reproduced from Ref. [5].

The masses and widths of the two tetraquark candidates observed for the first time are

$$\begin{aligned}
m(T^*_{c\bar{s}0}(2900)^0) &= 2.892 \pm 0.014 \pm 0.015\text{GeV},\\
\Gamma(T^*_{c\bar{s}0}(2900)^0) &= 0.119 \pm 0.026 \pm 0.013\text{GeV},\\
m(T^*_{c\bar{s}0}(2900)^{++}) &= 2.921 \pm 0.017 \pm 0.020\text{GeV},\\
\Gamma(T^*_{c\bar{s}0}(2900)^{++}) &= 0.137 \pm 0.032 \pm 0.017\text{GeV},
\end{aligned}$$

where the first uncertainties are statistical and the second systematic. The $T^*_{c\bar{s}}(2900)^0$ and $T^*_{c\bar{s}}(2900)^{++}$ states are observed in a simultaneous fit with 8σ and 6.5σ significance, respectively.

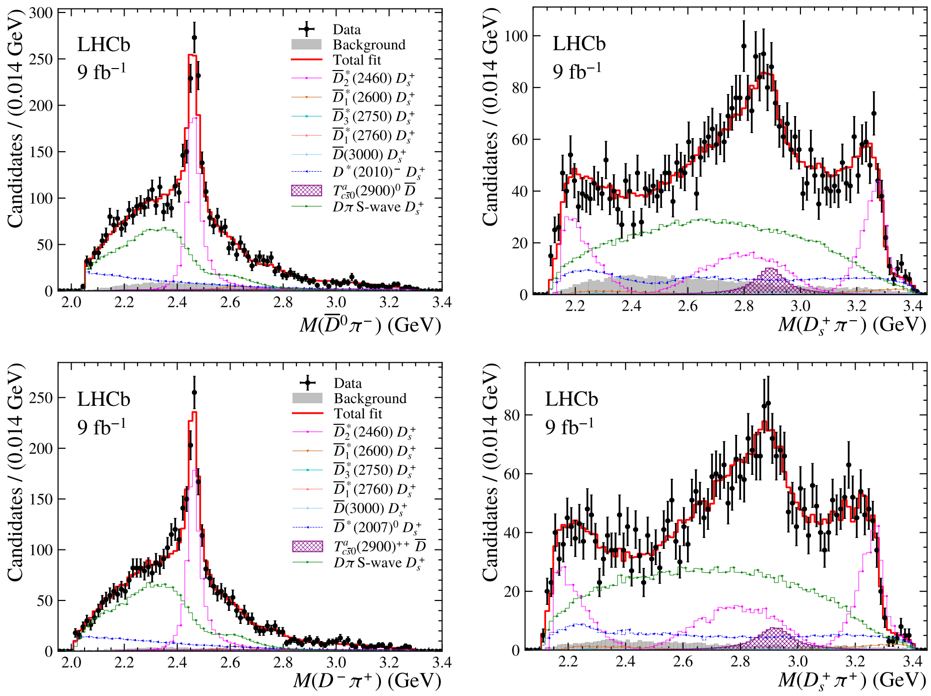

Figure 7: Fit projects of the full fit model for (top left) $m(\bar{D}^0\pi^-)$ and (top right) $m(D_s^+\pi^+)$ for $B^0 \to \bar{D}^0 D_s^+\pi^-$ decays, and (bottom left) $m(D^-\pi^+)$ and (bottom right) $m(D_s^+\pi^+)$ for $B^+ \to D^- D_s^+\pi^+$ decays for Run 1 and Run 2 datasets combined. Fit components are as described in the legend, reproduced from Ref. [5].

3.2 Amplitude analysis of $B^+ \to D^{*-}D_s^+\pi^+$ decays

The analysis of $B^+ \to D^{*-}D_s^+\pi^+$ decays [9] is motivated by the first observations of tetraquark candidates in Sec. 3.1, with a view to confirming the observations with an independent analysis of an alternative decay mode. The measurement uses the same Run 1 and Run 2 data samples and a similar B^+ meson decay process, with the addition of the $D^{*-} \to \bar{D}^0 \to K^+\pi^-$ decay channel.

The analysis follows closely that of the previous measurement [5, 6], with the dominant sources of background again being random combinations of tracks and candidates without two real charm mesons. These are again removed using a boosted decision tree algorithm and requirements on the flight distance, respectively. The fit to the B candidate invariant mass distribution is shown in Fig. 8 (left) and finds approximately 1000 signal events inside a 30 MeV window around the fitted B^+-meson mass. The distribution of candidates over the Dalitz plot is shown in Fig. 8 (right), note that this includes approximately 100 background events, giving a purity of around 90%.

The baseline amplitude model consists of just D^{**} mesons decaying in the $D^{*-}\pi^+$ channel, including the following states $D_1(2420)^0$, $D_1(2430)^0$, $D_2^*(2460)^0$, $D_1^*(2600)^0$, $D_2(2740)^0$ and $D_3^*(2750)^0$. The results of this fit are shown in Fig. 9 for projections in the (left) $m(D^{*-}\pi^+)$, (middle) $m(D_s^+\pi^+)$ and (right) $m(D^{*-}D_s^+)$ dimensions. The fit model reproduces the data distribution well in each projection, and in particular no clear discrepancies are seen in the $m(D_s^+\pi^+)$ plot where the tetraquark contribution would be expected.

In summary, no evidence is found for the presence of the $T_{c\bar{s}}^*(2900)^{++}$ in the $D_s^+\pi^+$ channel in $B^+ \to D^{*-}D_s^+\pi^+$ decays. An upper limit is calculated for its fit fraction, including systematic

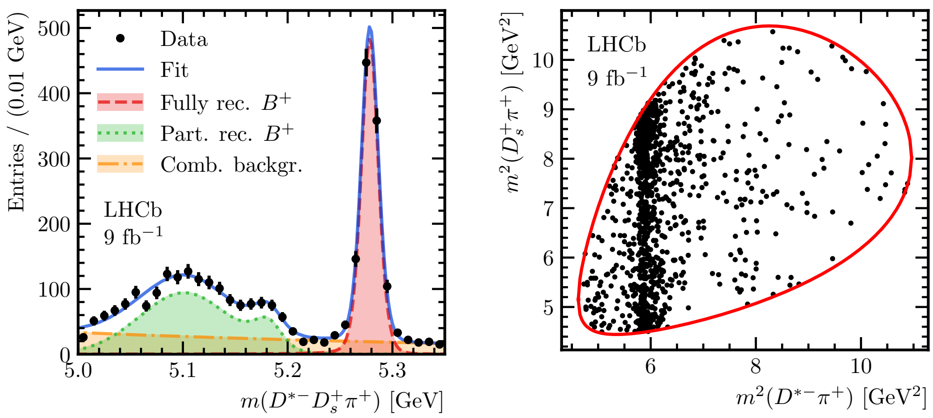

Figure 8: (Left) fit to the B candidate invariant mass distribution and (right) the Dalitz plot of candidates in a 30 MeV window around the known B-meson mass. Reproduced from Ref. [9].

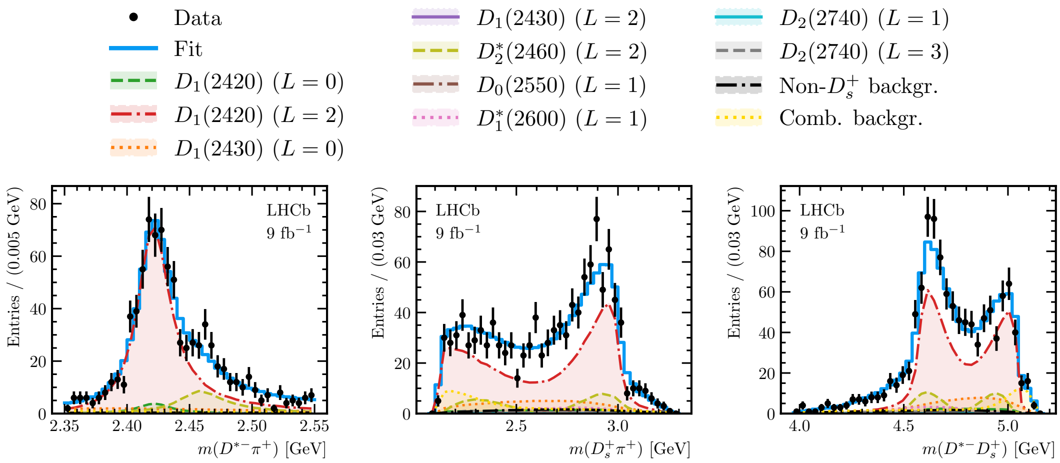

Figure 9: Projections of the amplitude fit to $B^+ \to D^{*-}D_s^+\pi^+$ candidates in (left) $m(D^{*-}\pi^+$, (middle) $m(D_s^+\pi^+$ and (right) $m(D*-D_s^+)$. The fit components are as described in the legend, reproduced from Ref. [9].

uncertainties, to be

$$\mathrm{FF}(T^*_{c\bar{s}}(2900)^{++}) < 2.3\,\%\ (90\,\%\mathrm{CL}).$$

3.3 Amplitude analysis of $B^+ \to D^{*\pm}D^{\mp}K^+$ decays

The analysis of $B^+ \to D^{*\pm}D^{\mp}K^+$ decays [10] is the most natural place to study the tetraquark candidates observed in $B^+ \to D^-D^+K^+$ decays [7, 8]. Both of the $B^+ \to D^{*-}D^+K^+$ and $B^+ \to D^{*+}D^-K^+$ final states are studied simultaneously because the contributions to the $D^{*-}D^+$ and $D^{*+}D^-$ channels are expected to be identical. The analysis uses the full Run 1 and Run 2 data samples. In the $B^+ \to D^{*+}D^-K^+$ channel tetraquark candidates might be expected in the D^-K^+ pair, while for $B^+ \to D^{*-}D^+K^+$ decays the $D^{*-}K^+$ pair is the relevant couple. Note that $T^*_{cs0}(2870)^0 \to D^{*-}K^+$ is forbidden by spin-parity conservation.

The main sources of background candidates are random combinations of tracks and candidates

Component	$J^{P(C)}$	Fit fraction [%] $B^+ \to D^{*+}D^-K^+$	Fit fraction [%] $B^+ \to D^{*-}D^+K^+$	Branching fraction $[10^{-4}]$
$\text{EFF}_{1^{++}}$	1^{++}	$10.9\,^{+2.3}_{-1.2}\,^{+1.6}_{-2.1}$	$9.9\,^{+2.1}_{-1.0}\,^{+1.4}_{-1.9}$	$0.74\,^{+0.16}_{-0.08}\,^{+0.11}_{-0.14} \pm 0.07$
$\eta_c(3945)$	0^{-+}	$3.4\,^{+0.5}_{-1.0}\,^{+1.9}_{-0.7}$	$3.1\,^{+0.5}_{-0.9}\,^{+1.7}_{-0.6}$	$0.23\,^{+0.04}_{-0.07}\,^{+0.13}_{-0.05} \pm 0.02$
$\chi_{c2}(3930)\,^{\dagger}$	2^{++}	$1.8\,^{+0.5}_{-0.4}\,^{+0.6}_{-1.2}$	$1.7\,^{+0.5}_{-0.4}\,^{+0.6}_{-1.1}$	$0.12\,^{+0.03}_{-0.03}\,^{+0.04}_{-0.08} \pm 0.01$
$\eta_c(3945)$	1^{+-}	$5.1\,^{+1.0}_{-0.8}\,^{+1.5}_{-0.8}$	$4.6\,^{+0.9}_{-0.7}\,^{+1.4}_{-0.7}$	$0.35\,^{+0.07}_{-0.05}\,^{+0.10}_{-0.05} \pm 0.03$
$\eta_c(3945)$	1^{++}	$10.1\,^{+1.6}_{-0.9}\,^{+1.3}_{-1.6}$	$9.1\,^{+1.4}_{-0.8}\,^{+1.2}_{-1.4}$	$0.69\,^{+0.11}_{-0.06}\,^{+0.09}_{-0.11} \pm 0.06$
$\psi(4040)\,^{\dagger}$	1^{--}	$2.8\,^{+0.5}_{-0.4}\,^{+0.5}_{-0.5}$	$2.6\,^{+0.5}_{-0.4}\,^{+0.4}_{-0.5}$	$0.19\,^{+0.04}_{-0.03}\,^{+0.03}_{-0.03} \pm 0.02$
$\eta_c(3945)$	1^{+-}	$1.2\,^{+0.2}_{-0.5}\,^{+0.2}_{-0.2}$	$1.1\,^{+0.2}_{-0.5}\,^{+0.2}_{-0.2}$	$0.08\,^{+0.01}_{-0.03}\,^{+0.02}_{-0.01} \pm 0.01$
$\eta_c(3945)\,^{\dagger}$	0^{+}	$6.5\,^{+0.9}_{-1.2}\,^{+1.3}_{-1.6}$	–	$0.45\,^{+0.06}_{-0.08}\,^{+0.09}_{-0.10} \pm 0.04$
$\eta_c(3945)\,^{\dagger}$	1^{-}	$5.5\,^{+1.1}_{-1.5}\,^{+2.4}_{-1.6}$	–	$0.38\,^{+0.07}_{-0.10}\,^{+0.16}_{-0.11} \pm 0.03$
$\text{NR}_{1^{--}}(D^{*\mp}D^{\pm})$	1^{--}	$20.4\,^{+2.3}_{-0.6}\,^{+2.1}_{-2.6}$	$18.5\,^{+2.1}_{-0.5}\,^{+1.9}_{-2.3}$	$1.39\,^{+0.16}_{-0.04}\,^{+0.14}_{-0.17} \pm 0.12$
$\text{NR}_{0^{--}}(D^{*\mp}D^{\pm})$	0^{--}	$1.2\,^{+0.6}_{-0.1}\,^{+0.7}_{-0.6}$	$1.1\,^{+0.6}_{-0.1}\,^{+0.6}_{-0.5}$	$0.08\,^{+0.04}_{-0.01}\,^{+0.05}_{-0.04} \pm 0.01$
$\text{NR}_{1^{++}}(D^{*\mp}D^{\pm})$	1^{++}	$17.8\,^{+1.9}_{-1.4}\,^{+3.6}_{-2.6}$	$16.1\,^{+1.7}_{-1.3}\,^{+3.3}_{-2.3}$	$1.21\,^{+0.13}_{-0.10}\,^{+0.24}_{-0.17} \pm 0.11$
$\text{NR}_{0^{-+}}(D^{*\mp}D^{\pm})$	0^{-+}	$15.9\,^{+3.3}_{-1.2}\,^{+3.3}_{-3.3}$	$14.5\,^{+3.0}_{-1.1}\,^{+3.0}_{-3.0}$	$1.09\,^{+0.23}_{-0.08}\,^{+0.22}_{-0.23} \pm 0.09$

Figure 10: Table of fit components from the amplitude analysis of $B^+ \to D^{*\pm}D^{\mp}K^+$ decays. The resulting fit fractions are presented and used to calculate the branching fraction for each component. Reproduced from Ref. [10].

without two real charm mesons. These are removed using a boosted decision tree algorithm and by requiring the charm mesons to have a significant flight distance with respect to the B meson decay vertex. After the selection requirements are applied, the purity of the sample in the signal mass window, 5260–5300 MeV, is approximately 95%. The signal yields are 1636 ± 43 for $B^+ \to D^{*+}D^-K^+$ decays and 1772 ± 44 for $B^+ \to D^{*-}D^+K^+$ decays.

The baseline fit for the amplitude analysis contains the components summarised in Fig. 10. To reach an acceptable level of agreement between the data and the fit model, a total of 13 components are required, including 4 new charmonium(-like) states ($\eta_c(3945)$, $h_c(4000)$, $\chi_{c1}(4010)$ and $h_c(4300)$) and two tetraquark contributions to $B^+ \to D^{*+}D^-K^+$ decays. It is interesting to note that no tetraquark contributions are found in the $D^{*-}K^+$ channel of $B^+ \to D^{*-}D^+K^+$ decays. Projections of the fit to both final states are shown in Fig. 11, where the fit quality is good, though some discrepancies are seen in $m(D^*D)$ (top). Such discrepancies are covered by systematic uncertainties from the model by including other known resonances ($\psi(4160)$, $\chi_{c1}(4160)$, $\psi(4415)$, and $\psi(4660)$) that do not significantly contribute to the baseline model.

In summary, two tetraquark candidates are required to accurately fit the $m(D^-K^+)$ distribution for $B^+ \to D^{*+}D^-K^+$ decays, in good agreement with previous results. Their masses and widths are found to be

$$
\begin{aligned}
m(T^*_{cs0}(2870)^0) &= 2.914 \pm 0.011 \pm 0.015\text{GeV}, \\
\Gamma(T^*_{cs0}(2870)^0) &= 0.128 \pm 0.022 \pm 0.023\text{GeV}, \\
m(T^*_{cs1}(2900)^0) &= 2.887 \pm 0.008 \pm 0.006\text{GeV}, \\
\Gamma(T^*_{cs1}(2900)^0) &= 0.092 \pm 0.016 \pm 0.016\text{GeV}.
\end{aligned}
$$

The $T^*_{cs0}(2870)^0$ states is observed at the 11σ level and the $T^*_{cs1}(2900)^0$ state at the 9.2σ level. For the four new charmonium(-like) states, the $\eta_c(3945)$ state is consistent with the $X(3940)$ state [11]

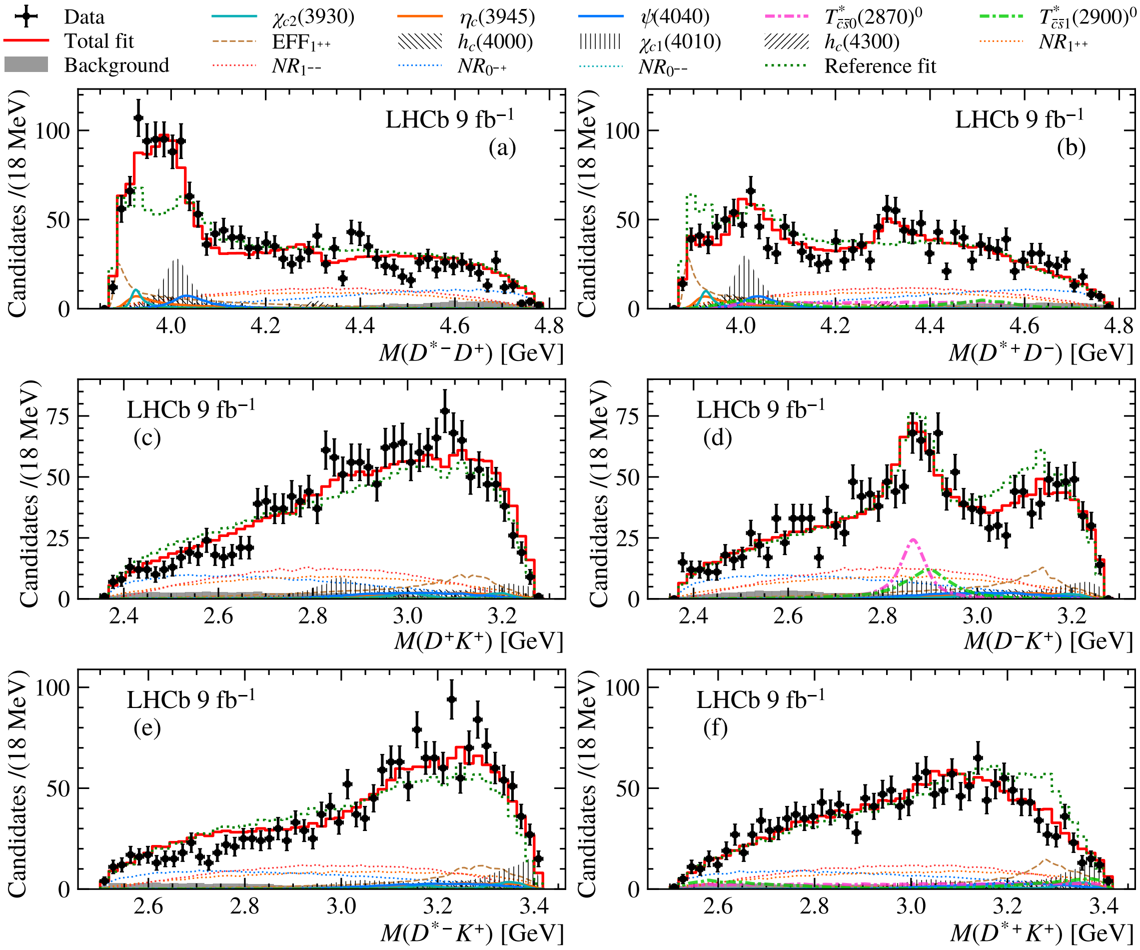

Figure 11: Projections of the simultaneous amplitude fit to the (left) $B^+ \to D^{*-}D^+K^+$ and (right) $B^+ \to D^{*+}D^-K^+$ data samples. The projection shown are (top) $D^{*\pm}D^{\mp}$, (middle) $D^{\pm}K^+$ and (bottom) $D^{*\pm}K^+$. Components are as described in the legend, reproduced from Ref. [10].

and the remaining three states are first observations above the 6σ level including systematics uncertainties with the following parameters

$$
\begin{aligned}
m(h_c(4000)) &= 4.000\,^{+0.017}_{-0.014}\,^{+0.029}_{-0.022}\,\text{GeV},\\
\Gamma(h_c(4000)) &= 0.182\,^{+0.071}_{-0.045}\,^{+0.097}_{-0.061}\,\text{GeV},\\
m(\chi_{c1}(4010)) &= 4.0125\,^{+0.0036}_{-0.0039}\,^{+0.0041}_{-0.0037}\,\text{GeV},\\
\Gamma(\chi_{c1}(4010)) &= 0.0627\,^{+0.0070}_{-0.0064}\,^{+0.0064}_{-0.0066}\,\text{GeV},\\
m(h_c(4300)) &= 4.3073\,^{+0.0064}_{-0.0066}\,^{+0.0033}_{-0.0041}\,\text{GeV},\\
\Gamma(h_c(4300)) &= 0.058\,^{+0.028}_{-0.016}\,^{+0.028}_{-0.025}\,\text{GeV},
\end{aligned}
$$

where the first uncertainties are statistical and the second systematic.

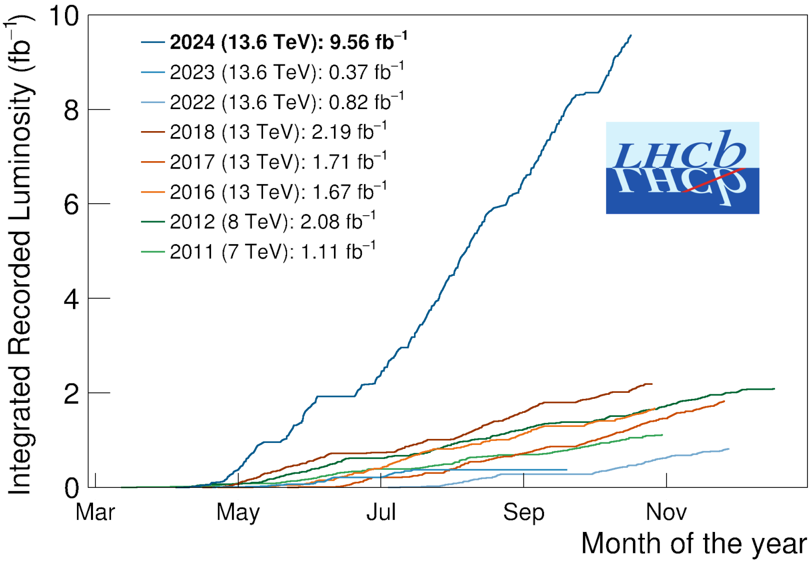

Figure 12: Accumulated luminosity recorded by the LHCb experiment during the years of operation, with 2024 (Run 3) in dark blue.

4. Future plans and summary

The future looks very bright for the LHCb experiment, the LHCb upgrade detector is performing well as it takes data during LHC Run 3. As shown in Fig. 12, the Run 3 dataset is already larger than those from Run 1 and Run 2 combined, with an additional factor of about two for hadronic B hadron decays per pb^{-1} from the removal of the hardware trigger. This means there are excellent prospects for updating the measurements presented here with the Run 3 data samples. Longer term, the LHCb Upgrade II proposal promises the ultimate precision on the LHCb physics programme and beyond, with an estimated sample size of 300 fb^{-1} [12].

References

[1] A. A. Alves, Jr. *et al.* [LHCb], *The LHCb Detector at the LHC*, JINST **3** (2008), S08005.

[2] R. Aaij *et al.* [LHCb], *Measurement of the branching fraction ratios $R(D^+)$ and $R(D^{*+})$ using muonic τ decays*, Phys. Rev. Lett. **134** (2025) 061801 [2406.03387].

[3] S. Banerjee *et al.* [HFLAV], *Averages of b-hadron, c-hadron, and τ-lepton properties as of 2023*, 2411.18639.

[4] R. Aaij *et al.* [LHCb], *List of hadrons observed at the LHC*, 2021, LHCB-FIGURE-2021-001.

[5] R. Aaij *et al.* [LHCb], *Amplitude analysis of $B^0 \to \overline{D}^0 D_s^+ \pi^-$ and $B^+ \to D^- D_s^+ \pi^+$ decays*, Phys. Rev. D **108** (2023) 012017 [2212.02717].

[6] R. Aaij *et al.* [LHCb], *First Observation of a Doubly Charged Tetraquark and Its Neutral Partner*, Phys. Rev. Lett. **131** (2023) 041902 [2212.02716].

[7] R. Aaij *et al.* [LHCb], *Amplitude analysis of the $B^+ \to D^+D^-K^+$ decay*, Phys. Rev. D **102** (2020), 112003 [2009.00026].

[8] R. Aaij *et al.* [LHCb], *A model-independent study of resonant structure in $B^+ \to D^+D^-K^+$ decays*, Phys. Rev. Lett. **125** (2020), 242001 [2009.00025].

[9] R. Aaij *et al.* [LHCb], *Amplitude analysis and branching fraction measurement of $B^+ \to D^{*-}D_s^+\pi^+$ decays*, JHEP **08** (2024), 165 [2405.00098].

[10] R. Aaij *et al.* [LHCb], *Observation of New Charmonium or Charmoniumlike States in $B^+ \to D^{*\pm}D^{\mp}K^+$ decays*, Phys. Rev. Lett. **133** (2024) 131902 [2406.03156].

[11] S. Navas *et al.* [Particle Data Group], *Review of particle physics*, Phys. Rev. D **110** (2024) 030001.

[12] R. Aaij *et al.* [LHCb], *Physics case for an LHCb Upgrade II - Opportunities in flavour physics, and beyond, in the HL-LHC era*, 1808.08865.